HHS Public Access

Author manuscript

J Comp Neurol. Author manuscript; available in PMC 2016 August 01.

Published in final edited form as:

J Comp Neurol. 2013 August 1; 521(11): 2551–2569. doi:10.1002/cne.23298.

Cell Death Atlas of the Postnatal Mouse Ventral Forebrain and Hypothalamus: Effects of Age and Sex

Todd H. Ahern[1,2,*], **Stefanie Krug**[2], **Audrey V. Carr**[2], **Elaine K. Murray**[2], **Emmett Fitzpatrick**[2], **Lynn Bengston**[2], **Jill McCutcheon**[2], **Geert J. De Vries**[2,3], and **Nancy G. Forger**[2,3,*]

[1]Center for Behavioral Neuroscience, Department of Psychology, Quinnipiac University, Hamden, Connecticut 06518

[2]Department of Psychology, Center for Neuroendocrine Studies, University of Massachusetts, Amherst, Massachusetts 01003

[3]Neuroscience Institute, Georgia State University, Atlanta, Georgia 30303

Abstract

Naturally occurring cell death is essential to the development of the mammalian nervous system. Although the importance of developmental cell death has been appreciated for decades, there is no comprehensive account of cell death across brain areas in the mouse. Moreover, several regional sex differences in cell death have been described for the ventral forebrain and hypothalamus, but it is not known how widespread the phenomenon is. We used immunohistochemical detection of activated caspase-3 to identify dying cells in the brains of male and female mice from postnatal day (P) 1 to P11. Cell death density, total number of dying cells, and regional volume were determined in 16 regions of the hypothalamus and ventral forebrain (the anterior hypothalamus, arcuate nucleus, anteroventral periventricular nucleus, medial preoptic nucleus, paraventricular nucleus, suprachiasmatic nucleus, and ventromedial nucleus of the hypothalamus; the basolateral, central, and medial amygdala; the lateral and principal nuclei of the bed nuclei of the stria terminalis; the caudate-putamen; the globus pallidus; the lateral septum; and the islands of Calleja). All regions showed a significant effect of age on cell death. The timing of peak cell death varied between P1 to P7, and the average rate of cell death varied tenfold among regions. Several significant sex differences in cell death and/or regional volume were detected. These data address large gaps in the developmental literature and suggest interesting region-specific differences in the prevalence and timing of cell death in the hypothalamus and ventral forebrain.

[*]CORRESPONDENCE TO: Nancy G. Forger, PhD, Petit Science Center, Georgia State University, Atlanta, GA 30302. nforger@gsu.edu; or Todd H. Ahern, Department of Psychology, Quinnipiac University, Hamden, CT 06518. todd.ahern@quinnipiac.edu.

CONFLICT OF INTEREST

The authors report no conflicts of interest.

ROLE OF AUTHORS

Study concept and design: THA, NGF. Acquisition of data: THA, SK, AVC, EKM, EF, LB, JM, NGF. Analysis and interpretation: THA, AVC, GJDV, NGF. Drafting of manuscript: THA, NGF. Critical revision of the manuscript for important intellectual content: THA, NGF. Statistical analysis: THA. Obtaining funding: NGF. Administrative, technical, and material support: THA, SK, EKM, JM, NGF. Study supervision: THA, NGF.

Keywords

activated caspase-3; sex differences

Cell death is a widespread and important feature of neural development. In vertebrates, approximately 50% of the neurons initially produced die by apoptosis, resulting in a profound reshaping of neural circuits (Clarke, 1985; Oppenheim, 1985). Although the concept of developmental neuronal cell death has been appreciated for decades, normative data in mammals are surprisingly spotty. One reason may be that much of the pioneering work in this field focused on nonmammalian models, most notably embryonic chicks and frogs (Oppenheim, 1981, 1985, 1991). In addition, many of the methods for detecting cell death, such as terminal deoxynucleotidyl transferase dUTP nick end labeling (TUNEL), are time consuming, making large-scale normative studies difficult.

More recently, rodents have gained prominence in the cell death literature and genetically modified mice have been extremely useful in molecular studies of apoptosis (Kuan et al., 2000; Strasser et al., 2011). Nonetheless, most current work focuses on injury-induced or disease-related neuronal death, rather than on naturally occurring neuronal cell death. During brain development, two phases of cell death have been described. Proliferative cell death takes place within the subventricular or ventricular zone and eliminates many neuronal precursor cells soon after they are generated; a second wave of cell death, often referred to as postmitotic cell death, takes place largely after neurons have migrated and begun to make axonal connections (Blaschke et al., 1996, 1998; Thomaidou et al., 1997; Kuan et al., 2000). Although it is clear that the bulk of postmitotic cell death takes place during the first postnatal week in both mice and rats, a detailed time course is available for relatively few brain regions. The lack of normative data is unfortunate because the postnatal cell death period identifies a time of vulnerability during which exposures to drugs, hormones, injury, infection, or variations in environmental factors such as maternal care are likely to have the greatest impact (McDonald et al., 1988; Ikonomidou et al., 1989, 1999; Yakovlev et al., 2001; Olney, 2002). Knowing where, and when, to look for effects of treatments or insults on postnatal cell death could greatly refine developmental studies.

Even in those regions where the pattern of developmental cell death has been reasonably well characterized, the effect of sex is generally unknown. Sex differences in neuron number in the sexually dimorphic nucleus of the preoptic area (SDN-POA) of rats, and the principal nucleus of the bed nucleus of the stria terminalis (BNSTp) in mice and rats, are attributed to sex differences in cell death during the neonatal period (Davis et al., 1996; Chung et al., 2000; Forger et al., 2004; Gotsiridze et al., 2007). Sex differences in developmental cell death in the visual cortex of rats have also been described (Nuñez et al., 2001), but few other brain regions have been examined in detail in both sexes. Recent studies suggest large-scale sex differences in neuronal vulnerability to hypoxia and other insults as well as sex differences in the molecular pathways underlying apoptosis induced by hypoxia–ischemia in adult and neonatal rodents (Hilton et al., 2003; Hagberg et al., 2004; Cheng and Hurn, 2010; Sharma et al., 2011). Whether these differences are specific to injury-induced death or also apply to naturally occurring cell death during development is unclear.

Developmental neuronal cell death is thought to depend primarily on the intrinsic, mitochondrial apoptosis pathway that is regulated by the Bcl-2 family of proteins. In response to a death signal, the pro-death family member Bax accumulates at the mitochondrial membrane, resulting in the release of signaling molecules such as cytochrome c (Yuan and Yankner, 2000; Roth and D'Sa, 2001). This in turn activates caspases, including the "executioner," caspase-3, which causes cellular demise through the cleavage of key intracellular proteins (Porter and Jänicke, 1999; Hengartner, 2000). The extrinsic cell death pathway that is initiated by signaling through cell surface death-receptors also culminates in the activation of caspase-3 (Porter and Jänicke, 1999). Activated caspase-3 (AC3) is therefore a good marker of dying cells in the developing nervous system. In comparison with other available methods (e.g., TUNEL) immunocytochemical detection of AC3 is rapid and robust and in our experience provides outstanding signal-to-noise throughout a range of antibody concentrations and other procedural modifications. Here we took advantage of these features to create a digitized, and therefore easily shared, "atlas" of cell death in the postnatal mouse brain. Below we report the first data from this project, focusing on cell death and volumetric changes in 16 regions through the ventral forebrain and hypothalamus in male and female mice from postnatal day (P) 1 through P11 (see Abbreviations for list of regions).

MATERIALS AND METHODS

Animals

General—All mice were housed in standard cages lined with Tekfresh bedding (7099; Harlan Laboratories) in a breeding colony at the University of Massachusetts, Amherst. Animals were maintained on a 14:10-hour light:dark cycle, and the temperature was held at 22°C. Food (a mix of 5001 and 5015; LabDiet) and water were available ad libitum. All procedures were approved by the University of Massachusetts, Amherst, IACUC and are in accordance with national guidelines.

Bax$^{-/-}$ and Bax$^{+/+}$ mice—*Bax* knockout (*Bax*$^{-/-}$) and *Bax* wild-type (*Bax*$^{+/+}$) pups were generated by mating males and females heterozygous for the *Bax* gene deletion (The Jackson Laboratory, Bar Harbor, ME). While originally generated on a C57BL/6 × 129 background (Knudson et al., 1995), these mice have been back-crossed to C57BL/6 for over 10 generations. *Bax*$^{-/-}$ and *Bax*$^{+/+}$ pups were collected on P2, P5, and P9 (birth = P0; two mice of each genotype at each age). Genotype was determined by PCR amplification of tail DNA using established primer sequences (White et al., 1998).

C57BL/6 mice for AC3 atlas—Eleven C57BL/6 breeder pairs were used to generate 135 pups. Pairs were checked at ~0900 hours and ~1430 hours each day for new litters, and the day of birth was designated P0. Pups were collected between 1400 and 1600 hours on P1 (12 females, 10 males), P3 (12 females, 12 males), P5 (12 females, 11 males), P7 (12 females, 11 males), P9 (12 females, 10 males), and P11 (12 females, 9 males). In most cases, no more than one male and one female were collected from each litter at a single time point.

Tissue collection and sectioning

Pups were rapidly decapitated, and brains were extracted and immersed in 5% acrolein fixative (90% acrolein [Sigma-Aldrich, St. Louis, MO; 110221] diluted in 0.1 M phosphate buffer [PB], pH 7.4) overnight. They were then transferred to 30% sucrose dissolved in 0.1 M PB and stored at 4°C. Coronal sections (40 μm) were collected from each animal using a freezing microtome, and sections were stored in cryoprotectant (30% sucrose, 1% polyvinylpyrrolidone, 30% ethylene glycol in 0.1 M PB) at −20°C until use.

Immunohistochemistry for AC3

Alternate sections from each animal were assayed for the presence of activated caspase-3 (AC3) using immunohistochemical detection with a commercially available antiserum (Table 1). Free-floating sections were agitated on a shaker for each of the following steps to keep the tissue from clumping, and steps were performed at room temperature unless otherwise noted. Sections were washed in 1× Tris-buffered saline (TBS; pH 7.6) for 3 × 5 minutes, then immersed in 1× TBS plus 0.0625 M sodium citrate for 30 minutes, washed again in 1× TBS for 3 × 5 minutes, and incubated in 1× TBS plus 0.1 M glycine for 30 minutes. The tissue was then washed in 1× TBS for 3 × 5 minutes and incubated in concentrated blocking solution (1× TBS, 20% normal goat serum, 0.3% Triton X [Fisher Scientific, Pittsburgh, PA; LC26280-1], and 1% hydrogen peroxide) for 30 minutes. Next, tissue was incubated in primary antibody solution (1:50,000 in 1× TBS, 2% normal goat serum, and 0.3% Triton X) overnight. The antibody concentration was based on the recommendations of the supplier as well as on data from a pilot study in which we ran a dilution curve.

On the next day, tissue sections were rinsed in dilute blocking solution (1× TBS, 1% normal goat serum, and 0.02% Triton X) for 3 × 10 minutes, incubated for 1 hour in a secondary antibody solution (1× TBS, 2% normal goat serum, 0.32% Triton X, goat anti-rabbit biotinylated secondary antibody diluted 1:250 [Vector, Burlingame, CA; BA-1000]), washed in 1× TBS plus 0.2% Triton X solution for 3 × 10 minutes, and then incubated in ABC solution (Vectastain ABC-Elite Kit; Vector) for 1 hour. The A and B components of the ABC kit were added to 1× TBS at a dilution of 1:100, based on pilot work for staining optimization. Next, the tissue was rinsed in 1× TBS for 3 × 15 minutes and developed for 7.5 minutes in commercial diaminobenzidine-nickel (DAB) solution (Vector; SK-4100). The tissue was then washed for >40 minutes in 1× TBS and stored at 4°C in 1× TBS until mounted on glass slides. Sections were counterstained with thionin (5.67 mM thionin acetate, 0.13% acetic acid, 5.67 mM sodium acetate anhydrous in dH_2O) for 10 seconds and differentiated (0.1% glacial acetic acid in 70% EtOH) for 40 seconds. Slides were then dehydrated, cleared in Hemo-De (Scientific Safety Solvents; HD-150) and coverslipped with Permount (Fisher Scientific).

Immunohistochemistry for AC3 and calbindin in the MPON

Twenty-one additional mice were collected on P5 (five females, five males) and P7 (five females, six males) to count AC3-labeled cells within the SDN-POA, a small subregion of the MPON that can be identified by calbindin immunostaining (Sickel and McCarthy, 2000; Edelmann et al., 2007; Gilmore et al., 2012). Brains were collected, sectioned as described

above, and assayed for the presence of AC3 and calbindin using immunohistochemical detection with the AC3 antibody described above and a commercially available calbindin antibody (Table 1).

The staining procedure mimicked that for AC3 labeling described above except that a 1:25,000 dilution of the cleaved caspase-3 antibody and a 1:500 dilution for the goat anti-rabbit secondary antibody were used. After completing the 7.5 minutes of development in the DAB-nickel solution to reveal AC3-labeled cells, the tissue was washed extensively and then incubated in calbindin primary antibody solution (1:10,000 antibody in 1× TBS, 2% normal goat serum, and 0.3% Triton X) overnight, followed by rinsing and exposure to secondary antibody (1:500 goat anti-mouse biotinylated secondary antibody [Vector; BA-9200] in 1× TBS, 2% normal goat serum, and 0.32% Triton X). Tissue was then developed for 3 minutes in DAB solution without nickel. Note that this procedure was intended not to double-label individual cells but to allow us to count AC3-labeled cells (black stain) within the calbindin-defined region of the MPON (identified by light brown cells and fibers).

Anitbody specificity

The activated caspase-3 antibody used here recognizes cleaved caspase-3 in human, mouse, and other species; detects a couplet on Western blots corresponding to a large (17/19 kDa) caspase-3 fragment; and does not cross-react with full-length (inactive) caspase-3 in human or mouse cells (Hu et al., 2000; Sammeta and McClintock, 2010, and manufacturer's data sheet). The calbindin antibody recognizes calbindin D-28K on immunoblots and does not react with other members of the EF-hand family such as calbindin D-9K, calretinin, myosin light chain, parvalbumin, S-100a, S-100b, S100A2 (S100L), and S100A6 (calcyclin; manufacturer's data sheet). Staining of mouse neurons by this antibody is abolished by preadsorbtion with the immunizing peptide (Gargini et al., 2007), and the pattern of staining seen in brain matches that seen with other calbindin antibodies (McClellan et al., 2010; and our observations).

Digital analysis of AC3-labeled regions of interest

All atlas slides were shipped to Olympus America Inc. (Center Valley, PA) and digitally scanned at 20× magnification using a NanoZoomer Digital Pathology slide scanner (Hamamatsu, Bridgewater, NJ). Digital images were then analyzed for AC3-labeled cells within defined regions of interest (ROIs; see Abbreviations) using Aperio's ImageScope viewer software (version 11.0.2.725).

Based on the thionin counterstain, each ROI was outlined in both hemispheres. ImageScope provided area measurements, and a trained rater counted the number of AC3-labeled cells within each tracing (see Fig. 1E). The sum of these counts was multiplied by 2 to correct for sampling ratio (i.e., every other section was immunostained) and is our measure of *total AC3-labeled cells* for each ROI. The estimated *regional volume* of each ROI was obtained by summing areas of all the sections for each ROI and then multiplying by section thickness and sampling ratio. *Cell death density* was calculated by dividing the total number of AC3-labeled cells in a given ROI by the regional volume and is expressed as number of AC3-

labeled cells per cubic millimeter. Cell death density is a measure frequently used in the cell death literature and allows for direct comparisons across multiple ROIs that differ markedly in regional volume.

For this study, we focused on 16 ROIs from the ventral forebrain and hypothalamus. We selected regions that could be reliably defined based on a Nissl stain in neonatal mice. In 14 of these ROIs, we traced every available section in which the structure was clearly visible. A mouse brain atlas (Paxinos and Franklin, 2008) was used to define structures as needed and to identify the Bregma levels reported below. For the GP, only the anterior portion was sampled, with boundaries extending from its first appearance rostrally to Bregma −0.34 mm. The CP and LS are very large structures, so we used a sampling procedure that allowed us to measure the same areas of these ROIs in each animal, independent of changes in volume with age. The CP was operationally defined as extending from Bregma 1.18 mm to −0.34 mm; the LS was operationally defined as extending from Bregma 1.10 mm to −0.46 mm. Four sections were then traced bilaterally in each animal, sampling the operational anterior boundary, the operational posterior boundary, and sections approximately one-third and two-thirds through the ROI. Thus, volumes reported below for the GP, CP, and LS do not represent the total ROI but should correspond to the same portion of the nucleus in each animal.

In addition to assessing specific ROIs, we also estimated overall forebrain growth from P1 to P11 by tracing the perimeter of the entire cross-section on every fifth section from Bregma 1.10 mm to −2.06 mm. This encompassed the rostrocaudal extent of the ROIs analyzed for this study.

GIMP 2.8 and Adobe Photoshop CS5.1 were used to create photomicrographs. GIMP 2.8 was used to crop images and adjust brightness and contrast. Photoshop was used to adjust vibrancy.

Statistical analysis

The number of AC3-labeled cells was compared in $Bax^{+/+}$ and $Bax^{-/-}$ mice by using an independent samples *t*-test. For the atlas, we conducted three separate two-way multivariate ANOVAs (MANOVAs) to control for type I error in our assessment of the effects of sex (male, female) and age (P1, P3, P5, P7, P9, P11) on cell death density, total number of AC3-labeled cells, and volume across our 16 ROIs. The MANOVAs revealed a global significant main effect of age for cell death density ($F_{4,57} = 4.97$, $P < 0.001$), total AC3 counts ($F_{4,57} = 3.80$, $P < 0.001$), and volume ($F_{4,57} = 2.06$, $P < 0.001$); they also revealed a global significant main effect of sex ($F_{1,57} = 3.29$, $P = 0.001$) and an age by sex interaction ($F_{4,57} = 1.44$, $P = 0.033$) for cell death density. Total AC3 counts and volume did not show a significant effect of sex ($F_{1,57} = 1.02$, $P = 0.458$, and $F_{1,57} = 1.45$, $P = 0.172$, respectively), although subject-wide exclusion criteria of the MANOVA (subjects with data missing in any variable are eliminated for all variables) greatly diminished the sample size of the MANOVAs. We followed each MANOVA with separate two-way ANOVAs examining the effects of age and sex for each ROI for each dependent variable: cell death density, total cell death, and regional volume. We focus on these analyses below. We also used separate two-

way ANOVAs to examine effects of sex on the density of AC3-labeled cells at P5 and P7 in the BNSTp, ICjM, and SDN-POA.

For the “heat maps” presented below, the two-way ANOVAs were followed by Tukey’s post hoc tests to identify homogenous data sets, and ages that did not differ statistically were depicted in the same color. For total AC3-labeled cells and cell death density, ages that statistically straddled two separate groupings were included in the group with the lower (more adult-like) rate of cell death; for volume, ages that straddled two separate groupings were included in the group with the larger (again, more adult-like) volume.

To assess the relationship between average cell death density and regional volume growth between P1 and P11, a Pearson’s correlation was calculated. All statistical analyses were conducted in SPSS 19.0.

RESULTS

Figure 1 depicts a digitally scanned slide from the C57Bl/6 atlas, shown at increasing magnifications. AC3-postive cells, many with neuronal-like processes, can clearly be seen at higher magnifications (Fig. 1C–E).

AC3 immunoreactivity labels Bax-dependent cell death

Deletion of the *Bax* gene virtually eliminates naturally occurring cell death in many regions of the embryonic and postnatal mouse brain as measured by TUNEL assay or the activation of caspase-3 (White et al., 1998; Srinivasan et al., 1998; Gotsiridze et al., 2007). To help validate the AC3 antibody used here, we compared AC3 labeling in $Bax^{+/+}$ and $Bax^{-/-}$ mice on postnatal days P2, P5, and P9. We found a near-elimination of AC3-labeled cells throughout the brains of $Bax^{-/-}$ mice at all three ages (see Fig. 2 for P2). Quantification suggests a reduction of about 95% of AC3 labeling in $Bax^{-/-}$ animals compared with controls (data not shown). Thus, the AC3 antibody used here reliably detects Bax-dependent cell death in the neonatal mouse brain.

Cell death and regional growth in the hypothalamus and forebrain

Sixteen ROIs in the hypothalamus and basal forebrain were analyzed for effects of age and sex on three dependent measures: AC3 cell density (also referred to below as “rate” of cell death), total number of AC3-labeled cells, and regional volume. Results of ANOVAs for the ROIs, as well as for our measure of whole brain volume, are presented in Table 2. There was a significant effect of age on all measures in all ROIs ($P < 0.001$ in each case). We found scattered effects of sex on cell death and regional volume and a single sex by age interaction. These effects are discussed further below.

Cell death density by age

Figure 3 presents cell death densities of all ROIs, collapsed for sex. In general, cell death density was higher at younger ages and declined with age; by P11, density was quite low in all regions, with the exception of the ICjM (Fig. 3C). However, the rate of cell death varied considerably across regions. In general, those areas with a low density of AC3-labeled cells

at P1 (e.g., BLA, CeA, and GP) continued to have low rates of cell death throughout the period analyzed.

Although a general pattern of declining cell death density with age is evident, several regions exhibited an inverted-U shape. For example, in agreement with a previous study (Gotsiridze et al., 2007), cell death density in the BNSTp increased from P1 to P5 before decreasing markedly between P5 and P11. The AVPV, ICjM, MPON, and SCN showed a similar pattern. The ICjM stood out in several respects, however. This cell group could not be detected in P1 animals and was apparent in only half of the animals on P3. The ICjM was also the only region we examined with appreciable cell death still in evidence at P11 (>400 AC3 cells/mm^3).

Total cell death and regional volume by age and sex

Cell death density is a function of the total number of dying cells in a region as well as changes in regional volume, which is expected to increase with age. We therefore also examined total cell death and volume for each of the ROIs, and these measures are plotted by sex in Figure 4. As with cell death density, the total number of dying cells generally decreased between P1 and P11 (Fig. 4); thus, decreases in cell death density are not simply a function of increasing volume. However, the peak of total number of AC3-labeled cells tended to be later than the peak for density (peak of total number of dying cells most often occurred between P3 and P5 and peak density between P1 and P3). Several ROIs showed a pattern of high cell death on P1, followed by a steady decrease (Arc, AVPV, BNSTl, GP, LS, MeA, and VMH), whereas the remaining regions showed some form of an inverted-U shape (AH, BLA, BNSTp, CeA, CP, ICjM, MPON, PVN, and SCN).

Not surprisingly, our measure of the “whole forebrain” (see Materials and Methods) as well as all regional volumes increased with age (Fig. 4). Whole-brain volume increased by 3.02-fold from P1 to P11, whereas growth in regional volumes varied in both magnitude and pattern (discussed further below). For example, the AVPV, Arc, BNSTl, and SCN showed little growth after P3, whereas the AH, CP, ICjM and all regions of the amygdala examined (BLA, CeA, and MeA) continued to show marked growth between P7 and P9.

Heat map of cell death suggests a transition at P5

Figure 5 presents “heat maps” depicting age-dependent changes in cell death density, total cell death, and volume in all ROIs, collapsed across sex. For this analysis, ages not statistically different from each other with respect to cell death density, total cell death, or volume for a given ROI are plotted in the same color. This allows for comparisons across structures and rapid visual identification of ages when cell death and volume growth are most vigorous. Figure 5A suggests a cell death “cliff” at P5: density of AC3-labeled cells declined significantly between P5 and P7 in 15 of the 16 ROIs. The only exception was the ICjM which, as mentioned above, appears to be developmentally phase-shifted to the right on several features. The heat map for the total number of AC3-labeled cells (Fig. 5B) also suggests an important transition between P5 and P7: 12 of the 16 regions were still exhibiting peak numbers of AC3 cells on P5 (red in heat map); this dropped to only three ROIs by P7.

Figure 6A presents average cell death density for each ROI, collapsed across both age and sex. The BLA had the lowest cell death density, averaging only 80 AC3-labeled cells/mm^3 from P1 to P11, which was less than half of the rate observed in the region with the next lowest cell death density. The AVPV, BNSTl, BNSTp, and ICjM had the highest densities, averaging between 650 and 890 AC3-labeled cells/mm^3. Thus, we observed a greater than tenfold variation across ROIs in the rate of cell death during the first 11 days of life.

We also assessed regional growth by calculating the fold change in volume in each ROI that was fully traced from P1 to P11; the CP and LS were excluded from this analysis because these structures were not assessed in their entirety (see Materials and Methods), and the ICjM was excluded because it was not present on P1. The Arc, AVPV, BNSTl, and SCN showed less than a doubling in size from P1 to P11 and therefore did not keep pace with total forebrain growth during this interval (dotted line in Fig. 6B), whereas the three amygdala regions examined (BLA, CeA, and MeA) each increased between 3.5- and 5.8-fold, thus outpacing overall forebrain growth (Fig. 6B).

To assess whether there was a relationship between cell death rate and regional growth, we performed a correlation of average cell death density and fold change in volume between P1 and P11. This revealed a significant negative correlation (Fig. 6C; Pearson's R = −0.672, P = 0.012), suggesting that the structures with greater cell death density grew at a slower rate.

Effects of sex

For most regions examined, density and total number of AC3-labeled cells were very similar between males and females. The P value for the main effect of sex on total number of AC3 cells, for example, ranged between 0.373 and 0.882 for 14 of the 16 regions (Table 2). We did, however, find a statistically significant effect of sex on total AC3-labeled cells (Fig. 4) and in density of AC3-labeled cells (data not shown) in the BNSTp (P < 0.014 and 0.0005, respectively), confirming previous reports that female mice display higher rates of developmental cell death in this region than do males (Gotsiridze et al., 2007; Broad et al., 2009; Wu et al., 2009). The expanded time course presented here further indicates that the sex difference is most pronounced on P5 and P7. The only other region in which the main effect of sex on cell death approached significance was the ICjM, in which males tended to have greater cell death between P1 and P11 than did females (P = 0.054 for density; P = 0.065 for total cell death). For this region, too, the difference appeared greatest on P5 and P7.

One of the regions where we might have expected to see sex differences in cell death is the MPON, because it contains the SDN-POA. Previous studies have indicated more cell death in the SDN-POA of female rats than of males during postnatal life (Davis et al., 1996; Chung et al., 2000). There was no sex difference in cell death density (P = 0.350, Table 2) or total AC3-labeled cells (P = 0.413) when the entire MPON was considered, although females tended to have slightly more dying cells than males beginning on P5. However, the SDN-POA occupies just a small subregion of the overall MPON, and this region can be identified based on calbindin immunoreactivity. We therefore labeled sections for both calbindin and AC3 and counted AC3 cells only within the calbindin-defined area, focusing on P5 and P7, based on previous studies of the SDN-POA of rats and the findings in the

BNSTp and ICjM described above. We found a sex difference in AC3 cell density, with females exhibiting more AC3 cells than males. Figure 7 compares the density of AC3-positive cells in the BNSTp, ICjM, and SDN-POA on P5 and P7; there is a significant sex difference in each case (BNSTp, female > male, $F_{1,40} = 17.05$, $P < 0.001$; ICjM, male > female, $F_{1,41} = 5.30$, $P = 0.026$; SDN-POA, female > male, $F_{1,17} = 7.77$, $P = 0.013$).

There was no effect of sex and no sex by age interaction on whole forebrain volume. However, sex differences in regional volumes were observed in the BLA, BNSTp, MeA, and MPON (main effect of sex in the two-way ANOVAs), and there was a sex by age interaction on volume of the SCN (Table 2). In the BLA and MeA, volumes were larger in males than females, although the absolute size difference was small and would likely be overlooked if investigated at only a single time point (Fig. 4). MPON volume was also greater in males in the overall ANOVA, and this appears to be due to a difference that emerged after P5 (Fig. 4).

DISCUSSION

We report here on naturally occurring cell death and volumetric changes in 16 regions of the mouse ventral forebrain and hypothalamus from P1 through P11. We find marked regional differences in the magnitude of cell death, with average AC3 density ranging more than tenfold, and peak cell death density ranging fivefold, across the brain areas examined. The density and total number of dying cells peaked between P1 and P7, depending on region, with the highest levels occurring early (P1) in the Arc, BLA, MeA, and BNSTl and late (P5–P7) in the BNSTp, ICjM, MPON, and SCN. The incidence of cell death was very low in all regions by P11, with the exception of the ICjM, where substantial cell death continued. As expected, measures of whole brain and regional volumes increased significantly during the first 11 postnatal days. However, the magnitude of the increase varied considerably: the AVPV, BNSTl, and SCN increased only about 1.5-fold during the first 11 days of life, whereas the BLA and CeA increased five- to sixfold during the same period. Interestingly, there was a significant negative correlation between cell death rate and volumetric change, suggesting that differences in cell death may contribute to relative volume differences.

The rate and timing of cell death were remarkably similar in both sexes for most regions examined, but females had more cell death than males in the BNSTp and a subregion of the MPON, and males tended to have more cell death than females in the ICjM. Sex differences appeared most pronounced on P5 and P7. There was no sex difference in overall brain size, but regional volume varied by sex in the BLA, BNSTp, MeA, and MPON (in all cases male > female).

Taken together, these data identify developmental differences among neighboring brain regions and support the value of an atlas-like approach, in which large numbers of regions are compared in a single study using identical methodology. The low cell death rates in the BLA and CeA, for example, might not be notable in a study focusing only on the amygdala but is striking in the context of a large number of other regions sampled across numerous time points. Similarly, by comparing the time course of cell death in multiple brain regions, a transition from high to lower rates of cell death was evident around P5 (the cell death “cliff” referred to above). Although the mechanism(s) underlying this transition is not

known, this suggests a common developmental switch that warrants further attention. The data presented here also may prove valuable for identifying brain regions and ages most likely to be affected by perinatal factors that impact developmental cell death. Several previous observations suggest that developing neurons may be more susceptible to perturbations during their cell death period (Ikonomidou et al., 1999; Mellios et al., 2009; Zacharaki et al., 2010); by extension, regions expressing very high or very low levels of postnatal cell death may exhibit different vulnerabilities.

Limitations

Our results reflect the true pattern of developmental neuronal cell death only to the extent that AC3 immunoreactivity reliably marks cells undergoing apoptosis. Although the activation of caspase-3 is considered a hallmark of apoptosis, nonapoptotic roles for caspase-3 have recently been described (e.g., in some forms of synaptic plasticity; Li et al., 2010; Hyman and Yuan, 2012). In previous studies of the perinatal rodent nervous system, however, most caspase-3-positive cells also showed signs of pyknosis (Srinivasan et al., 1998; Zacharaki et al., 2010; Zuloaga et al., 2011). Moreover, virtually all AC3 labeling was eliminated in *Bax*$^{-/-}$ mice in the present study. Thus, most of the cells labeled here were likely undergoing cell death.

The possibility that cells can undergo apoptosis without detectable activation of caspase-3 must also be considered; such cells would be missed in the current analysis. Caspase-independent cell death has been reported following neuronal injury (Zhan et al., 2001; Rideout and Stefanis, 2001; Cregan et al., 2002) and among dividing neuronal precursor cells (Lossi et al., 2004) but does not, as far as we are aware, normally occur during developmental cell death of postmitotic neurons. Cell death of postmitotic neurons can occur in knockout mice lacking caspase-3 or molecules upstream of caspase-3 (caspase-9 and Apaf-1; Oppenheim et al., 2001, 2008); however, the dying cells in this case display a nonapoptotic morphology that is not normally seen in wild-type animals.

As with other methods for quantifying cell death, AC3 immunoreactivity provides a snapshot of the number of cells in a particular stage of apoptosis at a given moment. Roughly 50% of the neurons initially produced undergo apoptosis (Oppenheim, 1991). Nonetheless, only a small fraction of cells are labeled at a given time using any available method of detecting apoptotic cells, because dying cells remain detectable in tissue sections only briefly before being cleared. Thus, the data presented here do not reveal the total number of cells eliminated by cell death in a given region, but comparisons of cell death across ages and regions should be valid, assuming a uniform clearance rate of dead cells. This is an assumption that is implicit in virtually all studies of cell death, but it is worth keeping in mind that clearance rates are difficult to measure and have only rarely been directly examined in vivo (for further discussion see Forger, 2006).

An additional consideration is that AC3 immunoreactivity alone cannot distinguish cell type, although several observations suggest that the large majority of labeled cells counted here were neurons. In our own experience, and consistent with that of others (e.g., Zuloaga et al., 2011), AC3-positive cells may not stain robustly for celltype specific markers such as NeuN, perhaps because the dying cells no longer express the antigen. Nonetheless, previous double-

label experiments indicate that most dying cells in the neonatal rodent brain are neuronal (Zacharaki et al., 2010; Zuloaga et al., 2011; Sophou et al., 2006). This is consistent with the fact that many AC3-positive cells in the current study had clear neuronal morphology and with the observation that that AC3 labeling was eliminated in *Bax*$^{-/-}$ mice. Postmitotic neurons require Bax for apoptosis, whereas the death of neural precursor cells and at least some glial cells occurs in the absence of Bax (White et al., 1998; Lindsten et al., 2003; Winseck and Oppenheim, 2006).

Regional differences in timing and rate of cell death

Many previous studies have examined cell death in specific regions of the postnatal mouse brain. The large majority of these, however, either have not been quantitative or have quantified cell death at only one or two postnatal ages. A relatively complete, quantitative time course has been available for only a few areas, including specific cell layers of the cerebellum, some regions of cerebral cortex, and cells of the substantia nigra pars compacta (Jackson-Lewis et al., 2000; Verney et al., 2000; Stankovski et al., 2007; Cheng et al., 2011); sex of the animals was not specified in any of these studies. Our findings are in general agreement with the previous reports, which show that cell death is observed primarily during the first 2 postnatal weeks in mice, with maximal rates of death observed during the first week of life. Previous studies have also found regional differences in both the rate and the timing of cell death. In the current study, the overall rate of cell death was highest in the AVPV, BNST (both BNSTp and BNSTl), and ICjM and was several-fold lower in the BLA, CeA, and GP. Peak numbers of dying cells were observed on P1 in some regions and up to 6 days later in others.

The cellular events that control regional differences in the rate and timing of developmental neuronal cell death are largely unknown. The available evidence does not support a close correspondence between the timing of cell birth and cell death across the regions examined here. For example, cells in the SDN-POA are born later than cells in the BNSTp, at least in rats (Bayer and Altman, 1987), yet both regions show a similar time course of cell death (Chung et al., 2000). The PVN ceases proliferation significantly earlier than the LS in the mouse (Creps, 1974; Karim and Sloper, 1980), but these two regions showed a very similar time course of cell death here. Similarly, the spatial/temporal sequence of cell death is unrelated to differences in the timing of neurogenesis between regions or cell layers the mouse neocortex (Verney et al., 2000). Thus, factors other than the time since final cell division likely determine the cell death period.

The molecular mechanisms underlying regional differences in the rate and timing of cell death also are not fully understood. The expression of several apoptosis-related genes is down-regulated in brain tissue after the postnatal period (Vekrellis et al., 1997; Shimohama et al., 1998; Krajewska et al., 2002; Zhu et al., 2005; Madden et al., 2007), which may serve to limit the cell death period and reduce susceptibility to insults later in life. The decreased expression of cell death genes may, in turn, be controlled by epigenetic modifications. For example, decreased histone acetylation in the promoter region of the caspase-3 gene is observed in whole-brain homogenates of rats on P60 compared with P2, which might contribute to the decreased expression of the caspase-3 gene in adults (Yakovlev et al.,

2010). The current data, which present a more fine-grained analysis of cell death in the hypothalamus and ventral forebrain than previously available, raise the question of whether there may be interesting regional differences in epigenetic marks that relate to either the overall magnitude or the timing of cell death.

Developmental cell death begins during embryonic life in the mouse brain. As mentioned above, large numbers of cells in the ventricular proliferative zones die soon after they are generated, and the death of postmitotic cells also begins prenatally. A high rate of cell death was seen on P1 in several of the ROIs examined here, which raises the question of whether peak cell death may occur prenatally in these regions. Although developmental cell death of some neuronal populations, such as spinal motoneurons, is primarily embryonic (see, e.g., Flanagan, 1969), this does not seem to apply to most brain regions. To the best of our knowledge, when neuronal cell death has been compared in a given brain region both pre- and postnatally within the same study, the highest rate of cell death has been seen at birth or later [e.g., basal forebrain (Sophou et al., 2006), dorsal lateral geniculate nucleus (Zacharaki et al., 2010), cerebellum (Cheng et al., 2011), somatosensory thalamus (Adams et al., 2004), olfactory bulb (Saito et al., 2004), substantia nigra (Oo and Burke, 1997), cerebral cortex and thalamus (Spreafico et al., 1995)]. Nonetheless, the regional differences that we observed in overall cell death rate were based only on postnatal cell death, and it is possible that relative rates would differ if both pre- and postnatal apoptosis were considered.

Effects of age and sex on regional volume

As expected, total brain size and volume of all ROIs increased significantly between P1 and P11. Our estimate of overall forebrain volume increased threefold over this interval, and individual regions increased from about 1.5-fold to 6-fold. We observed a significant negative correlation between rate of cell death and fold increase in volume, suggesting that volume increases are in part determined by the rate of cell death. The modest (1.6-fold) increase in SCN during the first 11 days of life seen here is consistent with what has been reported for hamsters (Müller and Torrealba, 1998). The most vigorous growth was seen in the BLA and CeA (5.8-fold and 4.7-fold increase in volume between P1 and P11, respectively). Similarly, the growth of these amygdala subdivisions outpaces overall brain growth during early postnatal life in primates (Chareyron et al., 2012), and vigorous postnatal growth of the BLA has been noted during the postnatal period in rats (Berdel et al., 1997).

Sex differences

An examination of sex differences in cell death and volumetric changes was also a major goal of the current study. For most of the regions that we examined, the rate of cell death in males and females was quite similar. The BNSTp showed greater cell death density as well as total AC3 cell number in females and greater volumes in males, which is consistent with previous observations in mice and rats (Chung et al., 2000; Gotsiridze et al., 2007; Broad et al., 2009; Wu et al., 2009). In adulthood, there is a sex difference in cell number and volume of the BNSTp of mice, which depends on the *Bax* gene and is regulated by estrogenic metabolites of testosterone acting early in life (Forger et al., 2004; Hisasue et al., 2010; Tsukahara et al., 2011).

An interesting, and previously unreported, sex difference in cell death in the ICjM was also suggested. Although the overall ANOVA found only near-significant trends for greater cell death density and total AC3 counts in males, an examination limited to P5 and P7 was significant. As far as we are aware, cell number in the ICjM of adult males and females has not been reported, so we do not know whether the sex difference in cell death (assuming that it can be verified in future studies) contributes to a sex difference in cell number or, alternatively, may compensate for a sex difference in neurogenesis.

The ICjM was also unusual in that it was not evident at birth and was identifiable only in about half of the animals at P3. This observation is consistent with reports that development of this region is protracted (Creps, 1974) and, specifically, with the finding that granule cell neurons of the islands of Calleja arise postnatally from a ventrally coursing offshoot of the rostral migratory stream (De Marchis et al., 2004). Cell death in the ICjM continued at a relatively high rate at the last age we examined here (>400 AC3 cells/mm^3 on P11), and the present material does not allow us to determine when cell death reaches adult-like levels. It is noteworthy that the two regions in which sex differences in cell death were suggested (the BNSTp and ICjM) also had relatively late peaks of cell death. Similarly, cell death is sexually dimorphic and peaks near the end of the first postnatal week in the SDN-POA of rats (Davis et al., 1996; Chung et al., 2000).

The findings presented here likely underestimate the extent of sex differences in cell death. Many of the ROIs that we examined were relatively large and comprised multiple subregions and cell types, and lack of significant sex differences overall does not mean that there are no sex differences for any cell group. This was in fact demonstrated in our analyses of the overall MPON and the portion of the MPON marked by calbindin immunoreactivity (the presumed SDN-POA). No significant sex difference in cell death density was found in the MPON overall, whereas an analysis limited to the calbindin-defined region demonstrated more dying cells in females than in males on P5 and P7.

We also might have missed sex differences based on the ages chosen for analysis. Because we collected brains on alternate days between P1 and P11, we would have missed any sex differences limited to days not sampled within that range or that occurred outside the range. The AVPV could be an example of the latter. The AVPV of rats and mice is larger in females than in males, and several lines of evidence support a role for cell death in the establishment of this sex difference (Murakami and Arai, 1989; Zup et al., 2003; Forger et al., 2004; Tsukahara et al., 2006; Waters and Simerly, 2009; Krishnan et al., 2009). Nonetheless, we did not find a significant sex difference in cell death in AVPV here. We note, however, that only two previous studies have directly compared the number of dying cells in AVPV in males and females, and both suggest that the sex difference may occur quite early. Sumida et al. (1993) found that male rats had a greater number of pyknotic cells in AVPV than females on embryonic day 21, and Tsukahara et al. (2006) found more caspase-3-positive cells in the AVPV of male rat pups than females at birth (P0). A sex difference in total number of thionin-stained cells in AVPV was also evident prenatally (Sumida et al., 1993). By contrast, as discussed above, sex differences in the BNSTp and SDN-POA are not present at birth and emerge at the end of the first postnatal week. Thus, it is possible that we missed a sex difference in AVPV cell death because it occurred earlier than was examined here. If so, this

suggests that the critical period for sexual differentiation of AVPV may close earlier than in regions such as the BNSTp and MPON. This is consistent with an observation in rats that the critical period for masculinization of the luteinizing hormone surge, a function controlled by AVPV, ends earlier than that for masculinization of SDN-POA morphology (Davis et al., 1995).

Several other sex differences in neuronal cell death have been reported. For example, Broad et al. (2009) found sex differences in AC3 cell density in a number of regions of the neonatal mouse brain, including the BNST, MeA, Arc, and other regions not examined here. In each case, the sex difference was limited to one of the two ages examined. Although we are in agreement with respect to a sex difference in cell death in the BNST, we did not find significant sex differences in cell death in the MeA or Arc. The reason for the different outcomes is not clear but may include differences between the two studies in the method of counting AC3 cells (Broad and colleagues used a grid to sample in multiple locations within each structure, whereas we counted throughout the entire structure), ages examined (P2 and P4 in the previous study vs. P1, P3, P5, P7, P9, and P11 here), or genotype [wild-type offspring of Peg3 heterogygotic pairs (Broad et al., 2009) vs. the C57Bl/6 mice used here].

Only a single sex by age interaction was found in the current study. Males had slightly higher SCN volumes on P1, P3, and P11 but lower volumes on P5, P7, and P9; although none of the individual comparisons was significant, this resulted in a sex by age interaction. The near-absence of sex by age interactions suggests that for most brain regions not only the overall *magnitude* but also the age-dependent *pattern* of cell death and volumetric change were very similar across sexes.

Sex differences in neuronal vulnerability (Hilton et al., 2003; Du et al., 2004, 2009) and in the molecular pathway underlying apoptosis after a toxic challenge have been described. In response to ischemia, for example, neurons of females tend to rely on a caspase-dependent pathway, whereas male neurons are more dependent on a pathway that is triggered by DNA repair enzymes and is largely caspase independent (Du et al., 2004; Hagberg et al., 2004; McCullough et al., 2005; Yuan et al., 2009; Liu et al., 2011; Cheng and Hurn, 2010). The current data suggest that this distinction does not apply to naturally occurring developmental cell death; if it did, sex differences in AC3 would be ubiquitous, which clearly was not the case. Because females had greater AC3 cell density only in the BNSTp and SDN-POA, two regions where females also have fewer neurons in adulthood, the sex difference in cell death is likely real and not offset by a caspase-independent pathway in males.

Together the data presented here demonstrate the utility of taking a more global approach to the study of cell death in the shaping of neural systems. Although sex does not exert widespread effects on developmental cell death, it does modify cell death in select regions and in a time-dependent manner. Such differences may contribute to established sex differences in behavior and in vulnerability to insult or disease.

ACKNOWLEDGMENTS

We thank Mike Veling for writing a Python program to collate data files.

Grant sponsor: National Institutes of Health; Grant number: R01-MH068482 (to N.G.F.); Grant number: T32-MH020051 (to T.H.A.).

Abbreviations

AH	anterior hypothalamus
Arc	arcuate nucleus
AVPV	anteroventral periventricular nucleus
BLA	basolateral amygdala
BNSTl	bed nucleus of the stria terminalis, lateral nucleus
BNSTp	bed nucleus of the stria terminalis, principal nucleus
CeA	central nucleus of the amygdala
CP	caudate-putamen
GP	globus pallidus
ICjM	islands of Calleja, major
LS	lateral septum
MeA	medial amygdala
MPON	medial preoptic nucleus
PVN	paraventricular nucleus of the hypothalamus
SCN	suprachiasmatic nucleus
SDN-POA	sexually dimorphic nucleus of the preoptic area
VMH	ventromedial nucleus of the hypothalamus

LITERATURE CITED

Adams SM, de Rivero Vaccari JC, Corriveau RA. Pronounced cell death in the absence of NMDA receptors in the developing somatosensory thalamus. J Neurosci. 2004; 24:9441–9450. [PubMed: 15496680]

Bayer SA, Altman J. Development of the preoptic area: time and site of origin, migratory routes, and settling patterns of its neurons. J Comp Neurol. 1987; 265:65–95. [PubMed: 3693605]

Berdel B, Moryś J, Maciejewska B, Dziewiatkowski J. Volume and topographical changes of the basolateral complex during the development of the rat's amygdaloid body. Fol Morphol. 1997; 56:1–11.

Blaschke AJ, Staley K, Chun J. Widespread programmed cell death in proliferative and postmitotic regions of the fetal cerebral cortex. Development. 1996; 122:1165–1174. [PubMed: 8620843]

Blaschke AJ, Weiner JA, Chun J. Programmed cell death is a universal feature of embryonic and postnatal neuroproliferative regions throughout the central nervous system. J Comp Neurol. 1998; 396:39–50. [PubMed: 9623886]

Broad KD, Curley JP, Keverne EB. Increased apoptosis during neonatal brain development underlies the adult behavioral deficits seen in mice lacking a functional paternally expressed gene 3 (*Peg3*). Dev Neurobiol. 2009; 69:314–325. [PubMed: 19224563]

Chareyron LJ, Lavenex PB, Amaral DG, Lavenex P. Postnatal development of the amygdala: a stereological study in macaque monkeys. J Comp Neurol. 2012; 520:1965–1984. [PubMed: 22173686]

Cheng J, Hurn PD. Sex shapes experimental ischemic brain injury. Steroids. 2010; 75:754–759. [PubMed: 19903490]

Cheng X-S, Li M-S, Du J, Jiang Q-Y, Wang L, Yan S-Y, Yu D-M, Deng J-B. Neuronal apoptosis in the developing cerebellum. Anat Histol Embryol. 2011; 40:21–27. [PubMed: 21231956]

Chung WC, Swaab DF, De Vries GJ. Apoptosis during sexual differentiation of the bed nucleus of the stria terminalis in the rat brain. J Neurobiol. 2000; 43:234–243. [PubMed: 10842236]

Clarke PG. Neuronal death in the development of the nervous system. Trends Neurosci. 1985; 8:345–349.

Cregan SP, Fortin A, MacLaurin JG, Callaghan SM, Cecconi F, Yu S-W, Dawson TM, Dawson VL, Park DS, Kroemer G, et al. Apoptosis-inducing factor is involved in the regulation of caspase-independent neuronal cell death. J Cell Biol. 2002; 158:507–517. [PubMed: 12147675]

Creps ES. Time of neuron origin in preoptic and septal areas of the mouse: an autoradiographic study. J Comp Neurol. 1974; 157:161–243. [PubMed: 4416651]

Davis EC, Shryne JE, Gorski RA. A revised critical period for the sexual differentiation of the sexually dimorphic nucleus of the preoptic area in rats. Neuroendocrinology. 1995; 62:579–585. [PubMed: 8751283]

Davis EC, Popper P, Gorski RA. The role of apoptosis in sexual differentiation of the rat sexually dimorphic nucleus of the preoptic area. Brain Res. 1996; 734:10–18. [PubMed: 8896803]

De Marchis S, Fasolo A, Puche AC. Subventricular zone-derived neuronal progenitors migrate into the subcortical forebrain of postnatal mice. J Comp Neurol. 2004; 476:290–300. [PubMed: 15269971]

Du L, Bayir H, Lai Y, Zhang X, Kochanek PM, Watkins SC, Graham SH, Clark RSB. Innate gender-based proclivity in response to cytotoxicity and programmed cell death pathway. J Biol Chem. 2004; 279:38563–38570. [PubMed: 15234982]

Du L, Hickey RW, Bayir H, Watkins SC, Tyurin VA, Guo F, Kochanek PM, Jenkins LW, Ren J, Gibson G, et al. Starving neurons show sex difference in autophagy. J Biol Chem. 2009; 284:2383–2396. [PubMed: 19036730]

Edelmann M, Wolfe C, Scordalakes EM, Rissman EF, Tobet S. Neuronal nitric oxide synthase and calbindin delineate sex differences in the developing hypothalamus and preoptic area. Dev Neurobiol. 2007; 67:1371–1381. [PubMed: 17638388]

Flanagan AE. Differentiation and degeneration in the motor horn of the foetal mouse. J Morphol. 1969; 129:281–305. [PubMed: 5343861]

Forger NG. Cell death and sexual differentiation of the nervous system. Neuroscience. 2006; 138:929–938. [PubMed: 16310316]

Forger NG, Rosen GJ, Waters EM, Jacob D, Simerly RB, de Vries GJ. Deletion of Bax eliminates sex differences in the mouse forebrain. Proc Natl Acad Sci U S A. 2004; 101:13666–13671. [PubMed: 15342910]

Gargini C, Terzibasi E, Mazzoni F, Strettoi E. Retinal organization in the retinal degeneration 10 (rd10) mutant mouse: a morphological and ERG study. J Comp Neurol. 2007; 500:222–238. [PubMed: 17111372]

Gilmore RF, Varnum MM, Forger NG. Effects of blocking developmental cell death on sexually dimorphic calbindin cell groups in the preoptic area and bed nucleus of the stria terminalis. Biol Sex Differ. 2012; 3:5. [PubMed: 22336348]

Gotsiridze T, Kang N, Jacob D, Forger NG. Development of sex differences in the principal nucleus of the bed nucleus of the stria terminalis of mice: role of Bax-dependent cell death. Dev Neurobiol. 2007; 67:355–362. [PubMed: 17443793]

Hagberg H, Wilson MA, Matsushita H, Zhu C, Lange M, Gustavsson M, Poitras MF, Dawson TM, Dawson VL, Northington F, et al. PARP-1 gene disruption in mice preferentially protects males from perinatal brain injury. J Neurochem. 2004; 90:1068–1075. [PubMed: 15312162]

Hengartner MO. The biochemistry of apoptosis. Nature. 2000; 407:770–776. [PubMed: 11048727]

Hilton GD, Nuñez JL, McCarthy MM. Sex differences in response to kainic acid and estradiol in the hippocampus of newborn rats. Neuroscience. 2003; 116:383–391. [PubMed: 12559094]

Hisasue S, Seney ML, Immerman E, Forger NG. Control of cell number in the bed nucleus of the stria terminalis of mice: role of testosterone metabolites and estrogen receptor subtypes. J Sex Med. 2010; 7:1401–1409. [PubMed: 20102443]

Hu BR, Liu CL, Ouyang Y, Blomgren K, Siesjø BK. Involvement of caspase-3 in cell death after hypoxia–ischemia declines during brain maturation. J Cereb Blood Flow Metab. 2000; 20:1294–300. [PubMed: 10994850]

Hyman BT, Yuan J. Apoptotic and non-apoptotic roles of caspases in neuronal physiology and pathophysiology. Nat Rev Neurosci. 2012; 13:395–406. [PubMed: 22595785]

Ikonomidou C, Mosinger JL, Salles KS, Labruyere J, Olney JW. Sensitivity of the developing rat brain to hypobaric/ ischemic damage parallels sensitivity to N-methyl-aspartate neurotoxicity. J Neurosci. 1989; 9:2809–2818. [PubMed: 2671294]

Ikonomidou C, Bosch F, Miksa M, Bittigau P, Vöckler J, Dikranian K, Tenkova TI, Stefovska V, Turski L, Olney JW. Blockade of NMDA receptors and apoptotic neurodegeneration in the developing brain. Science. 1999; 283:70–74. [PubMed: 9872743]

Jackson-Lewis V, Vila M, Djaldetti R, Guegan C, Liberatore G, Liu J, O'Malley KL, Burke RE, Przedborski S. Developmental cell death in dopaminergic neurons of the substantia nigra of mice. J Comp Neurol. 2000; 424:476–488. [PubMed: 10906714]

Karim MA, Sloper JC. Histogenesis of the supraoptic and paraventricular neurosecretory cells of the mouse hypothalamus. J Anat. 1980; 130:341–347. [PubMed: 7400041]

Knudson CM, Tung KS, Tourtellotte WG, Brown GA, Korsmeyer SJ. Bax-deficient mice with lymphoid hyperplasia and male germ cell death. Science. 1995; 270:96–99. [PubMed: 7569956]

Krajewska M, Mai JK, Zapata JM, Ashwell KWS, Schendel SL, Reed JC, Krajewski S. Dynamics of expression of apoptosis-regulatory proteins Bid, Bcl-2, Bcl-X, Bax and Bak during development of murine nervous system. Cell Death Differ. 2002; 9:145–157. [PubMed: 11840165]

Krishnan S, Intlekofer KA, Aggison LK, Petersen SL. Central role of TRAF-interacting protein in a new model of brain sexual differentiation. Proc Natl Acad Sci U S A. 2009; 106:16692–16697. [PubMed: 19805359]

Kuan CY, Roth KA, Flavell RA, Rakic P. Mechanisms of programmed cell death in the developing brain. Trends Neurosci. 2000; 23:291–297. [PubMed: 10856938]

Li Z, Jo J, Jia J-M, Lo S-C, Whitcomb DJ, Jiao S, Cho K, Sheng M. Caspase-3 activation via mitochondria is required for long-term depression and AMPA receptor internalization. Cell. 2010; 141:859–871. [PubMed: 20510932]

Lindsten T, Golden JA, Zong W-X, Minarcik J, Harris MH, Thompson CB. The proapoptotic activities of Bax and Bak limit the size of the neural stem cell pool. J Neurosci. 2003; 23:11112–11119. [PubMed: 14657169]

Liu Y, Young KA, Curtis JT, Aragona BJ, Wang Z. Social bonding decreases the rewarding properties of amphetamine through a dopamine D1 receptor-mediated mechanism. J Neurosci. 2011; 31:7960–7966. [PubMed: 21632917]

Lossi L, Tamagno I, Merighi A. Molecular morphology of neuronal apoptosis: analysis of caspase 3 activation during postnatal development of mouse cerebellar cortex. J Mol Histol. 2004; 35:621–629. [PubMed: 15614616]

Madden SD, Donovan M, Cotter TG. Key apoptosis regulating proteins are down-regulated during postnatal tissue development. Int J Dev Biol. 2007; 51:415–423. [PubMed: 17616931]

McClellan KM, Stratton MS, Tobet SA. Roles for gamma-aminobutyric acid in the development of the paraventricular nucleus of the hypothalamus. J Comp Neurol. 2010; 518:2710–2728. [PubMed: 20506472]

McCullough LD, Zeng Z, Blizzard KK, Debchoudhury I, Hurn PD. Ischemic nitric oxide and poly (ADP-ribose) polymerase-1 in cerebral ischemia: male toxicity, female protection. J Cereb Blood Flow Metab. 2005; 25:502–512. [PubMed: 15689952]

McDonald JW, Silverstein FS, Johnston MV. Neurotoxicity of N-methyl-D-aspartate is markedly enhanced in developing rat central nervous system. Brain Res. 1988; 459:200–203. [PubMed: 3048538]

Mellios K, Zacharaki T, Sophou S, Latsari M, Antonopoulos J, Dinopoulos A, Parnavelas JG, Dori I. Natural and lesion-induced apoptosis in the rat striatum during development. Brain Res. 2009; 1252:30–44. [PubMed: 19013438]

Müller C, Torrealba F. Postnatal development of neuron number and connections in the suprachiasmatic nucleus of the hamster. Brain Res Dev Brain Res. 1998; 110:203–213. [PubMed: 9748579]

Murakami S, Arai Y. Neuronal death in the developing sexually dimorphic periventricular nucleus of the preoptic area in the female rat: effect of neonatal androgen treatment. Neurosci Lett. 1989; 102:185–190. [PubMed: 2812498]

Nuñez JL, Lauschke DM, Juraska JM. Cell death in the development of the posterior cortex in male and female rats. J Comp Neurol. 2001; 436:32–41. [PubMed: 11413544]

Olney JW. New insights and new issues in developmental neurotoxicology. Neurotoxicology. 2002; 23:659–668. [PubMed: 12520755]

Oo TF, Burke RE. The time course of developmental cell death in phenotypically defined dopaminergic neurons of the substantia nigra. Brain Res Dev Brain Res. 1997; 98:191–196. [PubMed: 9051260]

Oppenheim, RW. Neuronal cell death and some related regressive phenomena during neurogenesis: a selective historical review and progress report. In: Cowan, WM., editor. Studies in developmental neurobiology: Essays in honor of Viktor Hamburger. Oxford University Press; New York: 1981. p. 480

Oppenheim RW. Naturally occurring cell death during neural development. Trends Neurosci. 1985; 8:487–493.

Oppenheim RW. Cell death during development of the nervous system. Annu Rev Neurosci. 1991; 14:453–501. [PubMed: 2031577]

Oppenheim RW, Flavell RA, Vinsant S, Prevette D, Kuan CY, Rakic P. Programmed cell death of developing mammalian neurons after genetic deletion of caspases. J Neurosci. 2001; 21:4752–4760. [PubMed: 11425902]

Oppenheim RW, Blomgren K, Ethell DW, Koike M, Komatsu M, Prevette D, Roth KA, Uchiyama Y, Vinsant S, Zhu C. Developing postmitotic mammalian neurons in vivo lacking Apaf-1 undergo programmed cell death by a caspase-independent, nonapoptotic pathway involving autophagy. J Neurosci. 2008; 28:1490–1497. [PubMed: 18256270]

Paxinos, G.; Franklin, KBJ. The coronal plates and diagrams. 3rd. Academic Press; San Diego: 2008. The mouse brain in stereotaxic coordinates, compact.

Porter AG, Jänicke RU. Emerging roles of caspase-3 in apoptosis. Cell Death Differ. 1999; 6:99–104. [PubMed: 10200555]

Rideout HJ, Stefanis L. Caspase inhibition: a potential therapeutic strategy in neurological diseases. Histol Histopathol. 2001; 16:895–908. [PubMed: 11510981]

Roth KA, D'Sa C. Apoptosis and brain development. Ment Retard Dev Disabil Res Rev. 2001; 7:261–266. [PubMed: 11754520]

Saito K, Saito S, Taniguchi K, Kobayashi N, Terashita T, Shimokawa T, Mominoki K, Miyawaki K, Chen J, Gao S-Y, et al. Transient increase of TUNEL-positive cells on postnatal day 20 in the developing rat olfactory bulb. Neurosci Res. 2004; 50:219–225. [PubMed: 15380329]

Sammeta N, McClintock TS. Chemical stress induces the unfolded protein response in olfactory sensory neurons. J Comp Neurol. 2010; 518:1825–1836. [PubMed: 20235094]

Sharma J, Nelluru G, Wilson MA, Johnston MV, Hossain MA. Sex-specific activation of cell death signalling pathways in cerebellar granule neurons exposed to oxygen glucose deprivation followed by reoxygenation. ASN Neuro [Internet]. 2011; 3 Available from: http://www.ncbi.nlm.nih.gov/pubmed/21382016.

Shimohama S, Fujimoto S, Sumida Y, Tanino H. Differential expression of rat brain bcl-2 family proteins in development and aging. Biochem Biophys Res Commun. 1998; 252:92–96. [PubMed: 9813151]

Sickel MJ, McCarthy MM. Calbindin-D28k immunoreactivity is a marker for a subdivision of the sexually dimorphic nucleus of the preoptic area of the rat: developmental profile and gonadal steroid modulation. J Neuroendocrinol. 2000; 12:397–402. [PubMed: 10792577]

Sophou S, Dori I, Antonopoulos J, Parnavelas JG, Dinopoulos A. Apoptosis in the rat basal forebrain during development and following lesions of connections. Eur J Neurosci. 2006; 24:573–585. [PubMed: 16903859]

Spreafico R, Frassoni C, Arcelli P, Selvaggio M, De Biasi S. In situ labeling of apoptotic cell death in the cerebral cortex and thalamus of rats during development. J Comp Neurol. 1995; 363:281–295. [PubMed: 8642075]

Srinivasan A, Roth KA, Sayers RO, Shindler KS, Wong AM, Fritz LC, Tomaselli KJ. In situ immunodetection of activated caspase-3 in apoptotic neurons in the developing nervous system. Cell Death Differ. 1998; 5:1004–1016. [PubMed: 9894607]

Stankovski L, Alvarez C, Ouimet T, Vitalis T, El-Hachimi KH, Price D, Deneris E, Gaspar P, Cases O. Developmental cell death is enhanced in the cerebral cortex of mice lacking the brain vesicular monoamine transporter. J Neurosci. 2007; 27:1315–1324. [PubMed: 17287506]

Strasser A, Cory S, Adams JM. Deciphering the rules of programmed cell death to improve therapy of cancer and other diseases. EMBO J. 2011; 30:3667–3683. [PubMed: 21863020]

Sumida H, Nishizuka M, Kano Y, Arai Y. Sex differences in the anteroventral periventricular nucleus of the preoptic area and in the related effects of androgen in prenatal rats. Neurosci Lett. 1993; 151:41–44. [PubMed: 8469435]

Thomaidou D, Mione MC, Cavanagh JF, Parnavelas JG. Apoptosis and its relation to the cell cycle in the developing cerebral cortex. J Neurosci. 1997; 17:1075–1085. [PubMed: 8994062]

Tsukahara S, Kakeyama M, Toyofuku Y. Sex differences in the level of Bcl-2 family proteins and caspase-3 activation in the sexually dimorphic nuclei of the preoptic area in postnatal rats. J Neurobiol. 2006; 66:1411–1419. [PubMed: 17013925]

Tsukahara S, Tsuda MC, Kurihara R, Kato Y, Kuroda Y, Nakata M, Xiao K, Nagata K, Toda K, Ogawa S. Effects of aromatase or estrogen receptor gene deletion on masculinization of the principal nucleus of the bed nucleus of the stria terminalis of mice. Neuroendocrinology. 2011; 94:137–147. [PubMed: 21525731]

Vekrellis K, McCarthy MJ, Watson A, Whitfield J, Rubin LL, Ham J. Bax promotes neuronal cell death and is downregulated during the development of the nervous system. Development. 1997; 124:1239–1249. [PubMed: 9102310]

Verney C, Takahashi T, Bhide PG, Nowakowski RS, Caviness VS Jr. Independent controls for neocortical neuron production and histogenetic cell death. Dev Neurosci. 2000; 22:125–138. [PubMed: 10657705]

Waters EM, Simerly RB. Estrogen induces caspase-dependent cell death during hypothalamic development. J Neurosci. 2009; 29:9714–9718. [PubMed: 19657024]

White FA, Keller-Peck CR, Knudson CM, Korsmeyer SJ, Snider WD. Widespread elimination of naturally occurring neuronal death in Bax-deficient mice. J Neurosci. 1998; 18:1428–1439. [PubMed: 9454852]

Winseck AK, Oppenheim RW. An in vivo analysis of Schwann cell programmed cell death in embryonic mice: the role of axons, glial growth factor, and the pro-apoptotic gene Bax. Eur J Neurosci. 2006; 24:2105–2117. [PubMed: 17042795]

Wu MV, Manoli DS, Fraser EJ, Coats JK, Tollkuhn J, Honda S-I, Harada N, Shah NM. Estrogen masculinizes neural pathways and sex-specific behaviors. Cell. 2009; 139:61–72. [PubMed: 19804754]

Yakovlev AG, Ota K, Wang G, Movsesyan V, Bao WL, Yoshihara K, Faden AI. Differential expression of apoptotic protease-activating factor-1 and caspase-3 genes and susceptibility to apoptosis during brain development and after traumatic brain injury. J Neurosci. 2001; 21:7439–7446. [PubMed: 11567033]

Yakovlev A, Khafizova M, Abdullaev Z, Loukinov D, Kondratyev A. Epigenetic regulation of caspase-3 gene expression in rat brain development. Gene. 2010; 450:103–108. [PubMed: 19909801]

Yuan J, Yankner BA. Apoptosis in the nervous system. Nature. 2000; 407:802–809. [PubMed: 11048732]

Yuan M, Siegel C, Zeng Z, Li J, Liu F, McCullough LD. Sex differences in the response to activation of the poly (ADP-ribose) polymerase pathway after experimental stroke. Exp Neurol. 2009; 217:210–218. [PubMed: 19268668]

Zacharaki T, Sophou S, Giannakopoulou A, Dinopoulos A, Antonopoulos J, Parnavelas JG, Dori I. Natural and lesion-induced apoptosis in the dorsal lateral geniculate nucleus during development. Brain Res. 2010; 1344:62–76. [PubMed: 20471376]

Zhan RZ, Wu C, Fujihara H, Taga K, Qi S, Naito M, Shimoji K. Both caspase-dependent and caspase-independent pathways may be involved in hippocampal CA1 neuronal death because of loss of cytochrome c From mitochondria in a rat forebrain ischemia model. J Cereb Blood Flow Metab. 2001; 21:529–540. [PubMed: 11333363]

Zhu C, Wang X, Xu F, Bahr BA, Shibata M, Uchiyama Y, Hagberg H, Blomgren K. The influence of age on apoptotic and other mechanisms of cell death after cerebral hypoxia-ischemia. Cell Death Differ. 2005; 12:162–176. [PubMed: 15592434]

Zuloaga DG, Carbone DL, Hiroi R, Chong DL, Handa RJ. Dexamethasone induces apoptosis in the developing rat amygdala in an age-, region-, and sex-specific manner. Neuroscience. 2011; 199:535–547. [PubMed: 22008524]

Zup SL, Carrier H, Waters EM, Tabor A, Bengston L, Rosen GJ, Simerly RB, Forger NG. Overexpression of bcl-2 reduces sex differences in neuron number in the brain and spinal cord. J Neurosci. 2003; 23:2357–2362. [PubMed: 12657695]

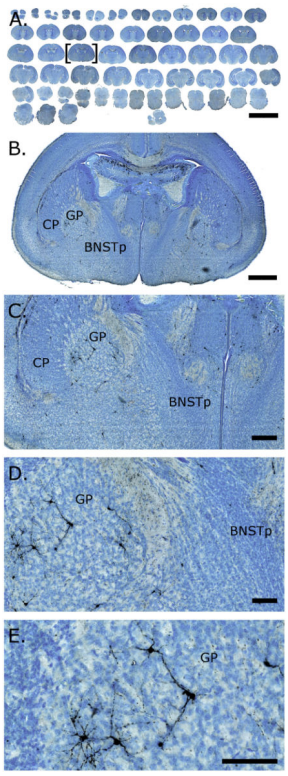

Figure 1.

Activated caspase-3 (AC3) immunoreactivity in digitally scanned brain sections from a postnatal day 1 mouse. Brains were labeled for AC3 and counterstained with thionin to assist in the identification of structures. Slides were digitally scanned, then images were opened and captured in ImageScope (Aperio). **A** depicts a low-power view of the entire scanned slide. **B–E** are progressively higher magnifications of the section marked by brackets in A. AC3-positive cells are clearly identifiable. Scale bars = 6 mm in A; 500 μm in B; 200 μm in C; 100 μm in D,E.

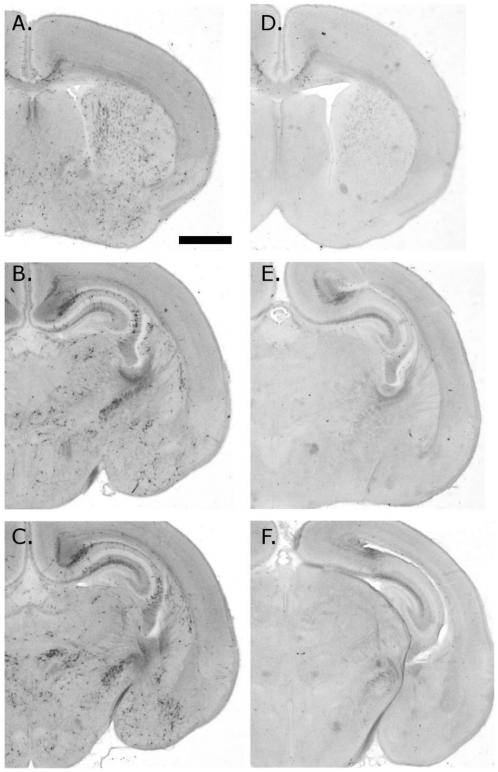

Figure 2.

Immunohistochemistry for activated caspase-3 (AC3) in wild-type ($Bax^{+/+}$) and *Bax* knockout ($Bax^{-/-}$) mice on postnatal day 2. Numerous AC3-labeled (black) cells are seen at all rostral–caudal levels of the forebrain in $Bax^{+/+}$ mice (**A–C** depict progressively more caudal sections of the same brain), whereas there is a near-elimination of this labeling in $Bax^{-/-}$ mice (**D–F**). The few AC3-labeled cells remaining in $Bax^{-/-}$ mice were found in the ventral cingulate cortex and corpus callosum region (D) and adjacent to the lateral ventricles (D–F). Scale bar = 1 mm.

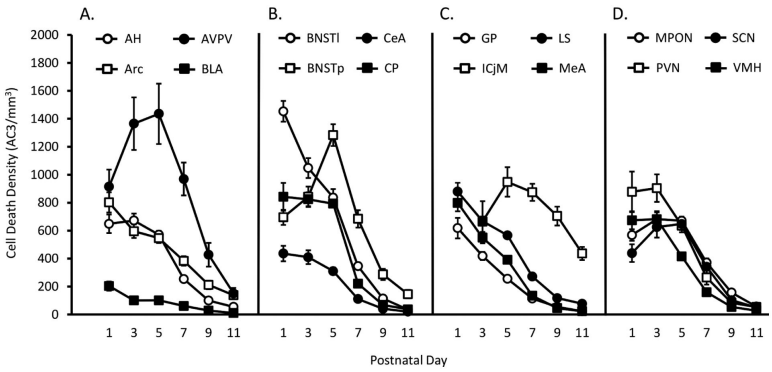

Figure 3.

Cell death density in 16 regions of the hypothalamus and ventral forebrain from postnatal days 1 to 11. Cell death density (number of activated caspase-3 [AC3]-labeled cells/mm^3) was measured on six postnatal days (P1, P3, P5, P7, P9, P11) in 16 regions of interest (ROIs). ROIs were grouped alphabetically and for ease of visualization are depicted in four separate graphs. **A:** Anterior hypothalamus (AH), arcuate nucleus (Arc), anteroventral periventricular nucleus (AVPV), and basolateral amygdala (BLA). **B:** Bed nucleus of the stria terminalis, lateral nucleus (BNSTl), bed nucleus of the stria terminalis, principal nucleus (BNSTp), central nucleus of the amygdala (CeA), and caudate-putamen (CP). **C:** Globus pallidus (GP), islands of Calleja, major (ICjM), lateral septum (LS), and medial amygdala (MeA). **D:** Medial preoptic nucleus (MPON), paraventricular nucleus of the hypothalamus (PVN), suprachiasmatic nucleus (SCN), and ventromedial nucleus of the hypothalamus (VMH).

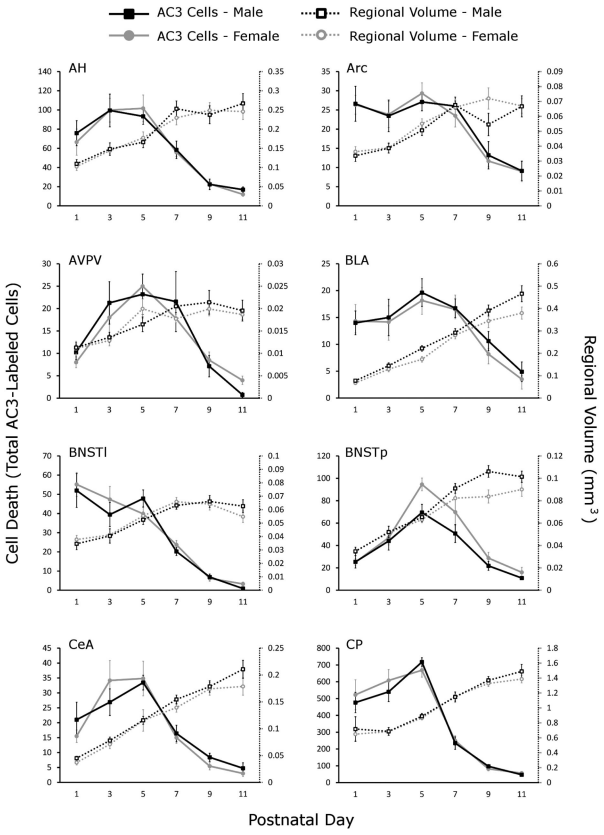

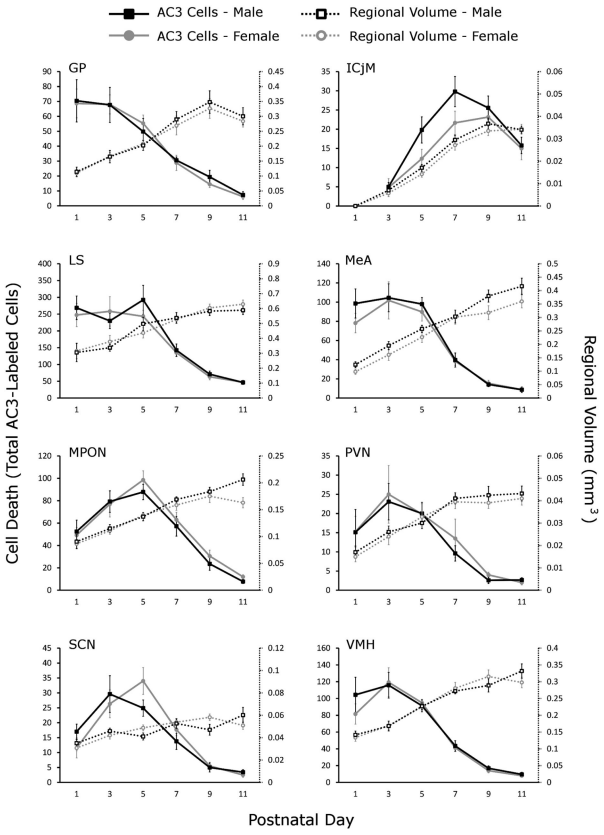

Figure 4.

Total number of activated caspase-3-labeled cells and regional volume by age and sex in 16 regions of interest. The total number of activated caspase-3 (AC3)-labeled cells (solid lines, y-axis on left) and the regional volume (dotted lines, y-axis on right) were graphed by sex (males in black, females in gray) and ordered alphabetically. For abbreviations see list.

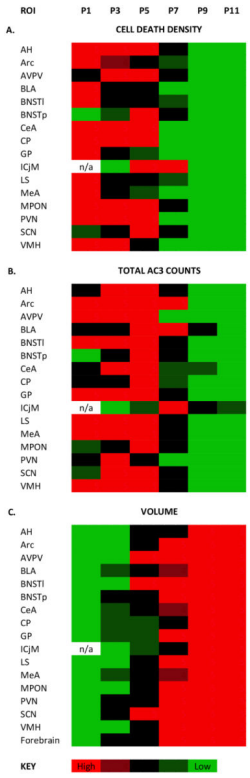

Figure 5.

Heat maps of cell death density, total cell death, and regional volume changes with age in 16 regions of interest. Within each region, data for males and females were combined, and Tukey's post hoc tests were used to compare cell death density (**A**), total number of activated caspase-3 (AC3)-labeled cells (**B**), or regional volume across ages (**C**). Ages with values that did not differ significantly from each other are the same color. High values are red, and progressively lower values move through black to green. P, postnatal day; ROI, region of interest; n/a, not assessed. See Materials and Methods for additional details.

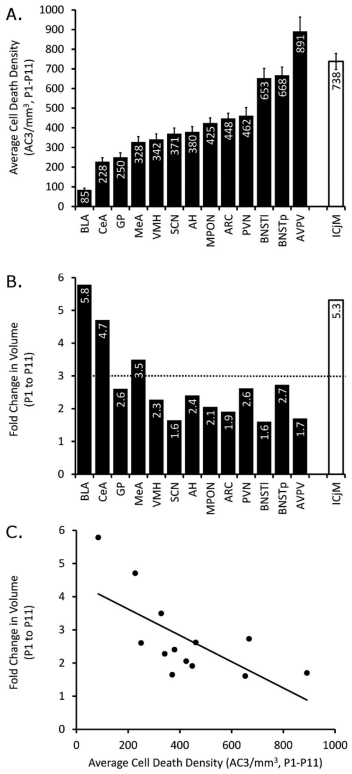

Figure 6.

Average cell death density and increases in volume vary by region and are negatively correlated. **A:** Cell death density averaged over both sex and age (P1, P3, P5, P7, P9, and P11) was calculated for each region of interest, and regions are ordered from lowest to highest density (left to right). The islands of Calleja (ICjM; white bar at right) is set apart because it was not discernible until P3; its average is based on P3–P11. **B:** The fold change in volume was also calculated and graphed, following the order of ROIs found in A. The dotted line indicates the fold change in "whole forebrain" volume from P1–P11. **C:** Average density and volume fold change were significantly negatively correlated (Pearson's R = −0.672, $P = 0.012$).

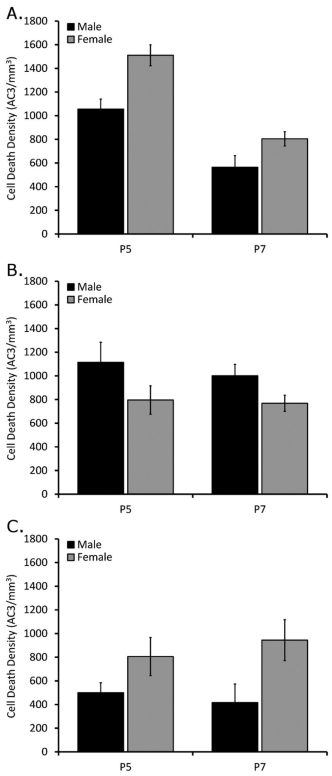

Figure 7.

The BNSTp, ICjM, and the calbindin-defined SDN-POA exhibit sex differences in cell death density across P5–P7. Females show greater rates of cell death in the principal nucleus of bed nucleus of the stria terminalis (BNSTp; $P < 0.001$; **A**) and sexually dimorphic nucleus of the preoptic area (SDN-POA; $P = 0.013$; **C**), whereas males show significantly greater rates in the islands of Calleja (ICjM; $P = 0.026$; **B**).

TABLE 1

Primary Antibodies

Antigen	Immunogen	Manufacturer data	Dilution
Activated caspase-3	Peptide sequence CRGTELDCGIETD, which is adjacent to Asp175 in human caspase-3	Cleaved caspase-3 antibody (polyclonal antibody raised in rabbit); Cell Signaling, 9661L, lot 36, Ref 08/2010	1:50,000
Calbindin D-28K	Purified bovine kidney calbindin D-28K	Anticalbindin D-28k antibody (monoclonal; derived from the CB-955 hybridoma produced by fusion of mouse myeloma cells and splenocytes from BALB/c mice immunized with purified bovine kidney calbinin D-28K); Sigma-Aldrich, C9848, lot 031M4859	1:10,000

TABLE 2

Results of Two-Way ANOVAs Examining Effects of Age and Sex on Cell Death Density, Total Cell Death, and Volume for the 16 Regions of Interest[1]

	CELL DEATH DENSITY						TOTAL AC3 COUNTS						VOLUME					
	Age		Sex		Age * Sex		Age		Sex		Age * Sex		Age		Sex		Age * Sex	
ROI	F	P-Value	F	P-Value	F	P-Value	F	P-Value	F	P-Value	F	P-Value	F	P-Value	F	P-Value	F	P-Value
AH	59.68	*0.000*	0.01	0.910	0.14	0.982	25.64	*0.000*	0.05	0.829	0.16	0.976	22.77	*0.000*	0.28	0.595	0.36	0.872
Arc	30.29	*0.000*	0.01	0.916	0.28	0.922	13.65	*0.000*	0.03	0.867	0.15	0.979	17.15	*0.000*	2.00	0.160	1.01	0.414
AVPV	11.93	*0.000*	0.17	0.678	0.53	0.756	12.57	*0.000*	0.06	0.812	0.38	0.858	11.44	*0.000*	0.23	0.632	0.95	0.454
BLA	18.65	*0.000*	0.62	0.433	0.28	0.922	9.55	*0.000*	0.52	0.470	0.08	0.995	95.12	*0.000*	10.47	*0.002*	1.16	0.331
BNSTI	114.68	*0.000*	0.07	0.796	1.43	0.218	41.25	*0.000*	0.26	0.614	0.68	0.643	18.59	*0.000*	0.00	0.991	0.53	0.750
BNSTp	52.71	*0.000*	13.64	*0.000*	1.93	0.094	29.03	*0.000*	6.27	*0.014*	1.10	0.362	40.16	*0.000*	5.60	*0.020*	1.22	0.306
CeA	28.97	*0.000*	0.18	0.676	0.33	0.896	20.31	*0.000*	0.05	0.824	0.69	0.631	52.95	*0.000*	2.83	0.095	0.46	0.807
CP	65.35	*0.000*	0.59	0.445	0.36	0.872	65.35	*0.000*	0.21	0.651	0.41	0.840	46.22	*0.000*	0.93	0.337	0.19	0.967
GP	45.12	*0.000*	0.06	0.810	0.08	0.995	26.68	*0.000*	0.02	0.882	0.12	0.988	25.86	*0.000*	0.47	0.495	0.12	0.987
ICjM	6.56	*0.000*	3.81	*0.054*	0.69	0.600	11.31	*0.000*	3.49	*0.065*	0.72	0.582	62.70	*0.000*	2.09	0.152	0.24	0.913
LS	112.41	*0.000*	2.32	0.131	0.62	0.684	31.60	*0.000*	0.42	0.517	0.57	0.723	22.73	*0.000*	0.11	0.739	0.64	0.668
MeA	90.86	*0.000*	0.28	0.601	0.12	0.989	34.68	*0.000*	0.80	0.373	0.32	0.902	48.47	*0.000*	8.42	*0.004*	0.53	0.755
MPON	52.38	*0.000*	0.88	0.350	0.22	0.952	31.96	*0.000*	0.68	0.413	0.25	0.939	35.80	*0.000*	4.84	*0.030*	1.60	0.166
PVN	28.16	*0.000*	0.82	0.368	0.37	0.870	10.14	*0.000*	0.22	0.637	0.09	0.993	22.34	*0.000*	0.67	0.415	0.27	0.929
SCN	25.59	*0.000*	0.04	0.836	0.32	0.902	23.56	*0.000*	0.12	0.733	1.32	0.262	11.00	*0.000*	0.05	0.828	2.47	*0.037*
VMH	70.03	*0.000*	0.12	0.733	0.09	0.993	38.96	*0.000*	0.40	0.531	0.45	0.814	49.82	*0.000*	0.02	0.878	0.90	0.482
Forebrain													62.01	*0.000*	0.42	0.520	0.40	0.850

[1] ROIs are listed alphabetically. Significant effects ($P < 0.05$) are highlighted in dark gray, and trends ($P < 0.1$) are highlighted in light gray to show global patterns.